

NOTES AND CORRESPONDENCE

Airborne Observations of Stratus Clouds During the Southerly Surge Event of 10 – 11 June 1994

JAMES W. ROTTMAN¹, STEVEN PLATNICK^{2,3*} AND MICHAEL D. KING³

¹*Science Applications International Corporation, San Diego, California*

²*University of Maryland Baltimore County, Baltimore, Maryland*

³*NASA Goddard Space Flight Center, Greenbelt, Maryland*

(submitted to *Monthly Weather Review* February 9, 1998)

* *Corresponding author address:* Dr. Steven Platnick, Code 913, NASA Goddard Space Flight Center, Greenbelt, MD, 20771 (E-mail: Platnick@climate.gsfc.nasa.gov)

1. Introduction

On 11 June 1994 during the Monterey Area Ship Track (MAST) experiment, which is summarized in Durkee et al. (1998), NASA's high altitude ER-2 aircraft imaged several distinct linear structures, not associated with ship tracks, in the low level stratus clouds over the ocean off the coast of central California. The images were obtained with the high spatial resolution MODIS Airborne Simulator (MAS) scanning spectrometer, King et al. (1996), which has narrowband spectral channels located from the visible through the thermal infrared. The small scale of these cloud structures (on the order of 100 m) is surprising, especially given the large spatial and time scales over which the observations were made, and therefore seems to be of potential importance to future cloud remote sensing efforts as well as cloud dynamical studies. It was later learned that the clouds in that region were associated with the decay phase of a so-called southerly surge event, also referred to as a coastally trapped disturbance or coastally trapped wind reversal. The dynamics of this relatively common event will be discussed in a later section. We begin with a discussion of the imagery and cloud remote sensing results.

The image shown in Fig. 1 was constructed from a series of images recorded over a period of 3.5 hours by the MAS on board the ER-2 as it flew the flight pattern shown in Fig. 2 over the Pacific Ocean just off the coast from Monterey Bay. The imagery shows a mostly uniform low-level layer of stratus clouds, but imbedded within this layer are sharp linear features that perhaps demarcate a boundary between two types of clouds or air masses. There is one very sharp boundary that is indicated by the arrow in the figure, and there are two or three less distinct boundaries further to the south. Note that the sharpest boundary appears to be moving towards the southwest, as indicated by the fact that in each flight line of the MAS image, which are separated in time by about 25 minutes, the line has moved approximately 12 to 15 km to the south.

Fig. 3 shows a close up image of the sharpest boundary. The location of this region is indicated in Fig. 1 by the arrow. The MAS has a spatial resolution of 50 m at nadir and from this image it can be seen that the width of the boundary seen in Fig. 1 is of this order, although in some places the boundary seems to consist of several parallel lines. The clouds on either side of this boundary appear to have similar cell structure. However, it is clear that the clouds to the north have less reflectivity than those to the south. On closer inspection there are indications of cloud streets. The streets are slightly more distinct to the north of the line. In addition, the axes of the streets are slightly different in the two regions. In the north the axis is nearly north-south, whereas in the southern region the axis is more northeast-southwest (cf. Fig. 1).

These observations were sufficiently intriguing to prompt an investigation into the origin of the cloud boundary. This note describes this investigation and its conclusions. Apparently the distinct boundaries in the stratus clouds observed by the ER-2 are in the region where two air masses came together during the decay phase of a southerly surge that occurred off the coast of California on 10–11 June 1994. Fortunately, another field experiment took place at the same time. This other experiment was part of the Coastal Meteorology Accelerated Research Initiative of the Office of Naval Research and was designed specifically to study the southerly surge that occurs along the California coast. We use the results of this experiment to elucidate the cause of the distinct cloud boundaries observed in the ER-2 imagery.

2. Microphysical analysis of the observations

a. MODIS Airborne Simulator (MAS)

The MODIS (MOderate resolution Imaging Spectroradiometer) Airborne Simulator (MAS) is a narrow band multichannel scanning spectrometer carried onboard NASA’s high altitude ER-2 aircraft. A detailed description of this instrument is given by King et al. (1996). For the observations made during MAST the data system was configured for 11 channels (subsequently upgraded to 50 channels in 1995) with 50 m resolution at nadir and flown on the ER-2 at a nominal altitude of 20 km and a speed of 200 m s⁻¹.

b. Cloud boundary advection velocity

The speed of propagation of the cloud boundary was derived from the adjacent ER-2 flight lines indicated in Fig. 1 (specifically the flight line indicated by the arrow and the one just to the east) assuming the direction of propagation was perpendicular to the boundary. Using this method the speed was determined to be approximately 7.5 m s⁻¹ in a south-east direction, about equivalent to the surface wind speed reported on that day.

c. Retrievals

Cloud optical thickness and effective radius can be retrieved from solar reflection measurements in the visible and near-infrared, where liquid water is non-absorbing and absorbing, respectively, as described in more detail, for example, by Twomey and Cocks (1989), Nakajima and King (1990) and Platnick and Twomey (1994). Cloud reflection measurements in the visible contain information primarily about optical thickness τ , whereas reflection measurements in the near-infrared contain information primarily about droplet size, since droplet absorption is proportional to effective radius ($r_e = \langle r^3 \rangle / \langle r^2 \rangle$), a

moment of the droplet size distribution that is useful for radiative transfer problems). For weakly absorbing channels, reflectance may also have a significant dependence on optical thickness.

MAS cloud retrievals were made for the indicated regions of Fig. 3 using the 0.67 μm channel for the non-absorbing channel. Choices for the absorbing channel include the 1.62, 2.13, and 3.74 μm MAS channels, each of which is located in an atmospheric window to limit atmospheric absorption. Liquid water absorption increases with wavelength such that the 1.62 μm channel has the least absorption, and therefore significant optical thickness dependency for the range of cloud thicknesses seen on the day of the observation. The 3.7 μm reflectance is the most absorbing and least dependent on optical thickness, but at this wavelength, cloud emission is significant and can dominate the solar component. However, cloud emission can be removed from the channel using thermal infrared estimates of cloud-top temperature. The 2.2 μm channel is somewhere between these two channels in usefulness. Retrievals using the visible channel in combination with each of the three near-infrared channels were made and compared with coordinated in situ cloud measurements obtained by the University of Washington C-131A on four days during the MAST experiment. On average, effective radius retrievals using the 1.6 and 2.2 μm channels are about 15-20% less than the expected size based on in situ measurements. This difference is within the uncertainty expected from MAS instrument calibration and the uncertainty in the physical model used for the radiative transfer calculations. Retrievals using the 3.7 μm channel gave sizes about 20-40% larger than expected. It was decided that retrievals using the 2.2 μm channel would be the better choice in analyzing the cloud boundary seen on 11 June 1994. Retrievals of cloud optical thickness and effective radius were made for several regions, from two different ER-2 flight lines, in the vicinity of the boundary. Results from one of these flight lines are shown in Figs. 3 and 4. Retrieval statistics are shown in Table 1. Details of MAS retrievals and validations made during the MAST experiment can be found in Platnick et al. (1998).

A significant difference is seen in the optical thickness and liquid water path (approximated as $\frac{2}{3} \tau r_e$). Both of these quantities are greater on the southern side than they are on the northern side of the observed boundary.

The 2.5 μm difference in effective radius also appears significant. However, size retrievals are subject to larger errors with the smaller optical thickness on the northern side of the boundary. Retrievals using the 3.7 μm channel, with less optical thickness dependency, show only a 1.5 μm size difference. Cloud-top temperature differences, derived from 3.7 μm retrievals, include the effect of surface emission transmitted through

the cloud in the thermal infrared ($11 \mu m$). The average cloud-top temperature difference across the boundary is insignificant.

We conclude that for the two sides of the sharp boundary observed in Fig. 1 there is a small but measurable difference in the cloud microphysical properties and large differences in the cloud optical thickness and reflectance. These measurable differences correspond with the larger scale structure in these two cloud regions.

Next, we turn to the meteorological question of the cause of these two cloud regions being in such sharp contact.

3. The Southerly Surge of 10-11 June 1994

The observations described above apparently occurred during the decay phase of a so-called “southerly surge” (also referred to as a coastally trapped disturbance or coastally trapped wind reversal) that was being observed at that time as part of the Coastal Meteorology Accelerated Research Initiative of the Office of Naval Research. These observations and their analyses are reported in Oosterling (1995), Persson et al. (1995, 1996), Dorman et al. (1997), Ralph et al. (1997) and Thompson et al. (1997).

The term southerly surge is used to describe a complex meteorological event that generally occurs once or twice a month during the summer along the west coast of the United States. The distinguishing feature of this event is the reversal of the predominantly northwesterly winds to southerlies within a zone approximately a hundred kilometers wide adjoining the coast and over a depth approximately 3–5 km above sea level. Associated with this wind reversal are an increase in the depth of the marine boundary layer, a rise in pressure, a decrease in temperature, and the formation of low-level stratus clouds and fog. The progression of the wind reversal up the coast can often be tracked in satellite imagery by following the associated wedge of low-level stratus cloud as it moves from the south to the north along the coast. For strong southerly surges, the transition to southerly flow is abrupt with the southerlies increasing to a speed of 15 m s^{-1} and near-surface temperatures decreasing by 10° C within a few minutes.

Analogous phenomena have been studied that occur around the southern end of Africa, as described by Gill (1977), and along the eastern coast of Australia, as described by Baines (1980) and Colquhoun et al. (1985), where the event is referred to as the “southerly burster”.

So far there are four theories for the southerly surge and its initiation. Originally Dorman (1985) suggested that the southerly surge is a form of solitary coastally trapped Kelvin wave. This is a large-scale wave in which buoyancy and Coriolis forces are impor-

tant and that requires the presence of a side boundary, such as the coastal mountains, for its existence. The wave is manifested as an isolated elevation of the marine boundary layer that propagates up the coast. The amplitude of the wave diminishes with distance away from the coast such that the wave is confined to within approximately a Rossby radius (80 – 100 km) of the coast. Other observations by Dorman (1987) and Mass et al. (1987) and numerical simulations, Klemp et al. (1994), suggest that some of the southerly surge events are more accurately described as a coastally trapped gravity currents. In this case a gravity current is initiated by a pool of dense, cool air in the south that propagates due to buoyancy forces into the less dense, warmer air to the north and is kept confined against the coastal mountains by Coriolis forces. The propagating front of a gravity current is much steeper than that of a wave and therefore the transition to southerly flow would be expected to be more abrupt.

Another proposal by Mass and Bond (1986) and Mass et al. (1996) is that the flow reversal is a mesoscale response to a synoptically forced along-shore pressure gradient. The along shore wind responds to this pressure gradient ageostrophically because it is blocked by the coastal topography. Finally, Persson et al. (1995, 1996) put forth the idea that the southerly wind is induced by a low-level plume of potential vorticity that is generated by friction due to an interaction between the offshore flow and coastal topography.

These four theories are not necessarily mutually exclusive. A theory that incorporates and unifies several of the theories described above is presented by Reason and Steyn (1992). This unified theory ascribes the initial perturbation of the marine boundary layer to synoptic conditions, such as flow towards the coast in the south and away from the coast in the north, but eventually this perturbation evolves into a solitary Kelvin wave. If the Kelvin wave is sufficiently large amplitude, it will develop a steep leading edge that could cause an abrupt change in the wind speed and which could be interpreted as an internal bore.

For the event of 10–11 June 1994, Oosterling (1995) has divided the evolution of the surge into four phases. In the first, or pre-initiation phase (0000 UTC 9 June – 0000 UTC 10 June), a thermally induced surface pressure trough over central California began to move towards the west and higher pressures began to ridge over southern California. In the second, or initiation phase (0600 UTC – 1200 UTC 10 June), the thermal trough moved off-shore in northern California and the higher pressures continued to develop in the south. Together these features produced a reversal of the along shore pressure gradient and the surge was initiated. In the third, or propagation phase (1500 UTC 10 June – 1200 UTC 11 June), the surge began propagating towards the north at a speed of 12 m s^{-1} , in

advance of a tongue of low-level stratus clouds. At the same time a mesoscale low pressure region developed off the central coast of California that promoted the progression of the surge. In the final, or decay phase (1500 UTC 11 June – 0000 UTC 12 June), the along shore pressure gradient returned to its normal direction and the winds shifted back to their normal northwesterly direction along the coast.

More details of what occurred during these different phases is described in the previously cited papers. It is interesting that there is some disagreement over which theoretical proposal best characterizes the southerly surge event of 10–11 June 1994. The observational analysis of Ralph et al. (1997) leads to the conclusion that the event most resembles a coastally trapped Kelvin wave that may have steepened into a shallowly sloped internal bore. However, the numerical simulations of this event by Thompson et al. (1997) leads to the contrary conclusion that this event best resembles a coastally trapped gravity current.

An important point in the present context is made by Ralph et al. (1997); this paper states that the tongue of low-level cloud that is commonly associated with the southerly surge, and often used as an indicator of the motion of the surge up the coast, are not coincident with the location of the wind reversal. In fact, the wind reversal precedes and travels at a faster speed than the cloud layer. For the case of the 10–11 June 1994 event the wind reversal propagated at a speed of 12 m s^{-1} whereas the tongue of stratus cloud was observed to propagate to the north at a speed of between 6 and 9 m s^{-1} .

4. The decay phase of 11 June 1994

The phenomena observed by the ER-2 at 1730 UTC – 2100 UTC 11 June occurred during the decay phase of the southerly surge, so we will focus on this phase of the event. Unfortunately, this phase of the southerly surge has not received much attention in the previous studies of this event.

In Fig. 5 we show a sequence of hourly visible images from the GOES-7 satellite for the period 1500 UTC – 2000 UTC 11 June. These images show the interaction of two distinct low-level cloud masses. The first comes from the south and is associated with the southerly surge. The second comes from the north and is associated with the restored northwesterly flow. At 1500 UTC these two cloud masses are in contact, just north of San Francisco bay, but there is still a distinct boundary between them. At the later times both cloud masses near the coast are compressed against the coastal topography by the synoptic forces re-establishing the northwesterly flow along to whole California coast.

A chart of sea-level pressure and station wind speeds in the region near the California

coast for 1500 UTC is shown in Fig. 6. This chart shows that the winds north of San Francisco Bay are indeed northwesterly, down the coast, and those south of the Bay are southerly along the coast. The point along the coast where the surface wind direction changes from northwesterly to southerly is approximately where the separate cloud masses are seen to be interacting in the 1500 UTC GOES image.

Looking again at Fig. 5, by 1800 UTC the northern and southern cloud masses have been forced together so that the boundary between them, visible as a dark band, has been stretched into a long gentle curve with an approximately southwesterly axis starting near San Francisco bay. The sharp boundary imaged by the ER-2 on this day at 2000 UTC is indicated by the arrow in Fig. 5 and is located to the northwest of the major cloud mass boundary. Note that a precursor to the ER-2 imaged boundary can be seen in the 1800 UTC image, although it does not appear as sharp as in the 2000 UTC image.

It seems reasonable to assume that air mass from the north and the air mass from the south interact and mix just off the coast from San Francisco bay and Monterey bay. Evidence of this mixing is manifested by the considerable structure visible in the stratus clouds in this region. Since the wind reversal actually propagates ahead of the low-level clouds associated with the southerly surge, we speculate that the boundary imaged by the ER-2 is a result of the air from the south mixing with the air from the north to modify the microphysical and thermodynamical structure of the clouds in this area.

What is remarkable is that these microphysical and optical thickness differences are measurable and that the boundary line imaged by the ER-2 remains so sharp over several hundred kilometers (Fig. 5) and for the approximate half-hour over which the ER-2 observations were made (Fig. 1). Without a detailed model study, we cannot determine the specific mechanism that maintains this sharp boundary. However, we can say that the formation of the boundary is associated with the decay of the southerly surge and the re-establishment of the northwesterly flow. To that extent, satellite observations of such distinct cloud features would be expected to be relatively common off the coast of California during southerly surge events.

Acknowledgments. We thank F. M. Ralph at the NOAA/ERL Environmental Technology Laboratory, Boulder, CO and William T. Thompson at the Naval Research Laboratory, Monterey, CA for sharing their observational data and model results with us, Wendell Nuss at the Naval Postgraduate School, Monterey, CA for providing us with a copy of P.S. Oosterling's M.S. thesis, and Kathleen Strabala at the University of Wisconsin/CIMSS for assistance in reading the GOES data files. The relevance of the Southerly Surge to the observations described here came from discussions with Chaing Chen at the

NASA Goddard Space Flight Center, Greenbelt, MD. This work was funded by the U.S. Office of Naval Research under contracts N00014-92-C-0184 and N00014-95-F-0022.

REFERENCES

- Baines, P.G., 1980: The dynamics of the southerly burster. *Aust. Meteor. Mag.*, **28** 175-200.
- Colquhoun, J.R., D.J. Shepherd, C.E. Coulman, R.K. Smith and K. McInnes, 1985: The southerly burster of south eastern Australia: an orographically forced cold front. *Mon. Wea. Rev.*, **113** 2090 – 2107.
- Dorman, C. E., 1985: Evidence of Kelvin waves in California’s marine layer and related eddy generation. *Mon. Wea. Rev.*, **113**, 827–839.
- , 1987: Possible role of gravity currents in northern California’s coastal summer wind reversals. *J. Geophys. Res.*, **92**, 1497–1506.
- , L. Armi, J.M. Bane, and D. Rodgers 1997: Surface mixed layer during the 10-11 June 1994 California coastally trapped event. *Mon. Wea. Rev.*, to appear.
- Durkee, P.A., K.J. Noone and R.T. Bluth, 1998: The Monterey Area Ship Track (MAST) Experiment. *J. Atmos. Sci.*, submitted.
- Gill, A.E., 1977: Coastally trapped waves in the atmosphere. *Quart. J. Roy. Meteorol. Soc.*, **103**, 431–440.
- King, M. D., W. P. Menzel, P. S. Grant, J. S. Myers, G. T. Arnold, S. E. Platnick, L. E. Gumley, S. C. Tsay, C. C. Moeller, M. Fitzgerald, K. S. Brown and F. G. Osterwisch, 1996: Airborne scanning spectrometer for remote sensing of cloud, aerosol, water vapor and surface properties. *J. Atmos. Oceanic Technol.*, **13**, 777–794.
- Klemp, J. B., R. Rotunno, and W. C. Skamarock, 1994: Propagation of atmospheric gravity currents along the coastal barrier. In *Proc. Sixth Conf. On Mesoscale Processes*, Portland, OR, Amer. Meteor. Soc., 497–500.
- Mass, C. F. and M. D. Albright, 1987: Coastal southerlies and alongshore surges of the West Coast of North America: Evidence of mesoscale topographically trapped response to synoptic forcing. *Mon. Wea. Rev.*, **115**, 1707–1738.
- and N. A. Bond, 1986: Coastally trapped wind reversals along the United States West Coast during the warm season. Part II: Synoptic evolution. *Mon. Wea. Rev.*, **124**, 446–451.
- , ——— and D.J. Brees, 1996: The onshore surge of marine air into the Pacific Northwest: A coastal region of complex terrain. *Mon. Wea. Rev.*, **114**, 2602–2627.
- Nakajima, T., and M. D. King, 1990: Determination of the optical thickness and effective particle radius of clouds from reflected solar radiation measurements. Part I: Theory. *J. Atmos. Sci.*, **47**, 1878–1893.

- Oosterling, P.S., 1995: *Coastally trapped disturbances along the U.S. West Coast: Synoptic and mesoscale analysis of 9-12 June 1994*. M.S. thesis, Naval Postgraduate School, Monterey, CA, 73 pp. [Available from Department of Meteorology, Naval Postgraduate School, Monterey, CA 93043-5000.]
- Persson, P.O.G., P.J. Neiman, and F.M. Ralph, 1995: Topographically generated potential vorticity anomalies: A proposed mechanism for initiating coastally trapped disturbances. Preprints, *Seventh Conf. on Mountain Meteorology*, Breckenridge, CO, Amer. Meteor. Soc., 216–222.
- , ——, and ——, 1996: The role of a topographically generated potential vorticity anomaly in initiating a coastal wind reversal. Preprints, *Conf. on Coastal Oceanic and Atmospheric Prediction*, Atlanta, GA, Amer. Meteor. Soc., 120–124.
- Platnick, S., P. A. Durkee, K. Nielson, J. P. Taylor, S.-C. Tsay, M. D. King, and J.W. Rottman, 1998: The role of background cloud microphysics in the radiative formation of ship tracks. *J. Atmos. Sci.*, To appear.
- and S. Twomey, 1994: Determining the susceptibility of cloud albedo to changes in droplet concentration with the advanced very high resolution radiometer. *J. Appl. Met.*, **33**, 334–347.
- Ralph, F.M., L. Armi, J.M. Bane, C. Dorman, W.D. Neff, P.J. Neiman, W. Nuss, and P.O.G. Persson, 1997: Observations and analysis of the 10-11 June 1994 coastally trapped disturbance. *Mon. Wea. Rev.*, submitted.
- Reason, C. J. C. and D. G. Steyn, 1992: The dynamics of coastally trapped mesoscale ridges in the lower atmosphere. *J. Atmos. Sci.*, **49**, 1677–1692.
- Thompson, W. T., T. Haack, J. D. Doyle, and S. D. Burk, 1997: A nonhydrostatic mesoscale simulation of the 10-11 June 1994 coastally trapped wind reversal. *Mon. Wea. Rev.*, **125**, 3211–3230.
- Twomey, S., and T. Cocks, 1989: Remote sensing of cloud parameters from spectral reflectance in the near-infrared. *Beitr. Phys. Atmos.*, **62**, 172–179.

Table 1. Statistics of cloud retrievals for the regions indicated by the boxes in Fig. 3

Location (relative to boundary in Fig. 3)	Average optical thickness	Standard deviation	Average effective radius (μm)	Standard deviation	Average liquid water path ($g m^{-2}$)	Average cloud-top temperature (K)
	$\langle \tau \rangle$	σ_{τ}	$\langle r_e \rangle$	σ_{r_e}		
North side	9.8	1.7	4.6	1.0	31	281.7
South side	15.8	2.7	7.0	0.2	74	281.5

Figure Captions

FIG. 1 Large-scale cloud region, imaged by the MODIS Airborne Simulator (MAS) 0.67 μm channel, off the coast of Monterey Bay, California on 11 June 1994 from 1730 to 2100 UTC. The cloud boundary, shown in more detail in Fig. 3, is indicated by the arrow. Each ER-2 flight line represents about a 25 minute offset (earlier flight lines to the east) accounting for the discontinuity seen in the cloud boundary between adjacent flight lines.

FIG. 2. The flight path of the ER-2 on 11 June 1994 corresponding to the image in Fig. 1. The arrows indicate the direction of travel of the aircraft and the labels refer to the time of overpass in UTC.

FIG. 3. Cloud boundary imaged with the MAS 0.67 μm channel on 11 June 1994 (ER-2 flight line indicated on Fig. 1). The image area is 35 km across the scan line (horizontal) by about 33 km along the direction of flight (vertical). The image has not been spatially resampled so pixels away from nadir along the scan direction cover larger distances. The regions enclosed by boxes were used for the cloud retrievals discussed in the text.

FIG. 4. Retrievals of cloud optical thickness and effective radius made using the MAS 0.67 and 2.13 μm channels on the two sides of the cloud boundary shown in Fig. 3 at 2013 UTC. The histograms were generated from retrievals made over regions of about 7.75 km by 5.0 km as indicated by the boxes in Fig. 3.

FIG. 5. A sequence of three GOES-7 images at 1500, 1800 and 2000 UTC on 11 June 1994 showing the decay phase of the southerly surge. The approximate position of the ER-2 at 2000 UTC is indicated in the image by the arrow.

FIG. 6. Isobars of sea-level pressure (solid lines, 1 mb intervals) for 1500 UTC 11 June 1994 near the coast of Monterey Bay, California. The region shown is approximately equal to that in Fig. 5 and the heavy dashed line indicates the approximate eastern edge of the cloud layer visible at 1500 UTC in Fig. 5. Also shown are selected ship and buoy observations of surface wind speed; a full wind barb represents 5 m s^{-1} and a half wind barb 2.5 m s^{-1} . This figure is adapted from Fig. 20 in Oosterling (1995), where more information is given about the multiquadratic technique used to blend the available pressure measurements into the gridded fields of the National Meteorological Center mesoscale ETA model.

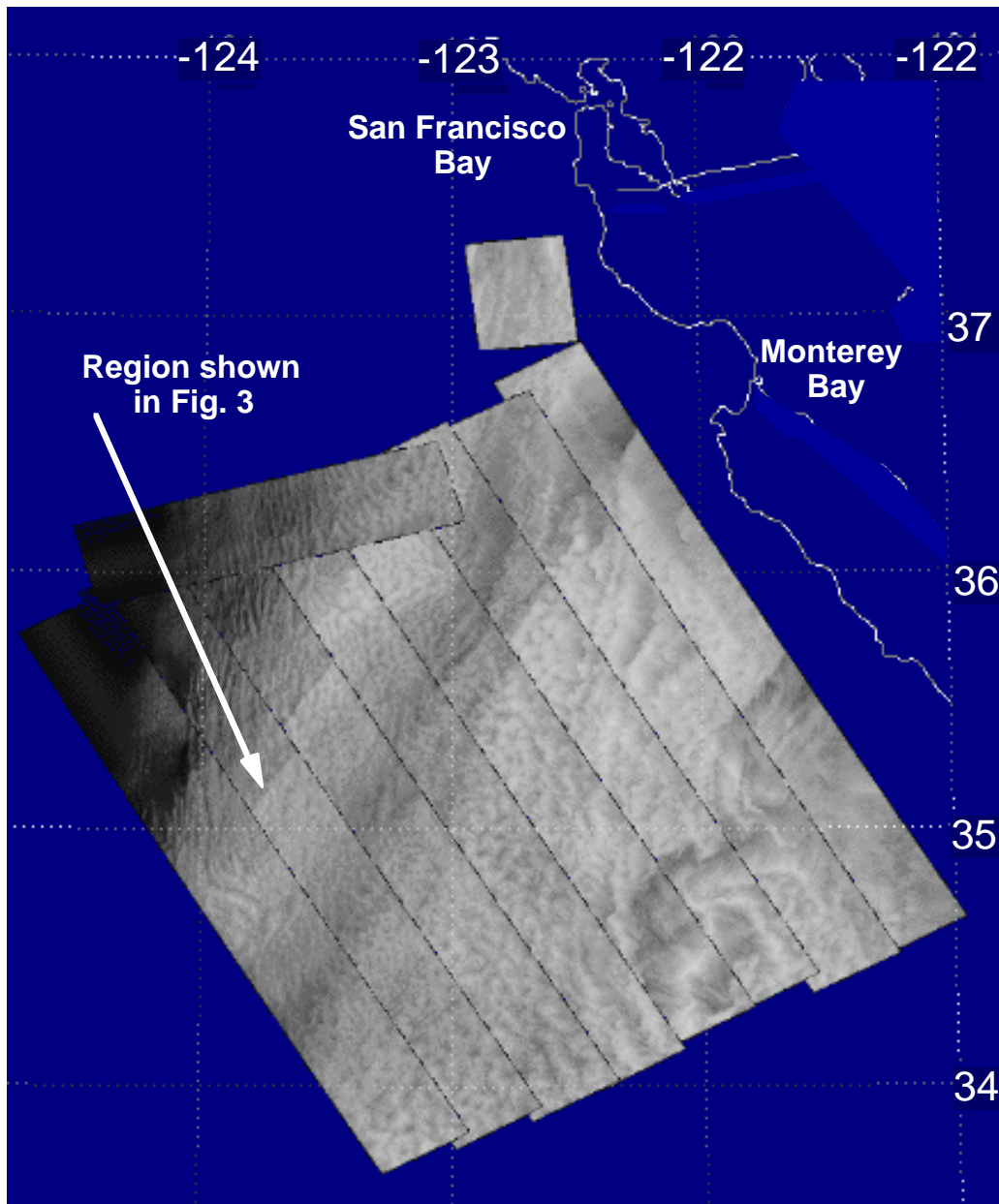


Fig. 1. Large-scale cloud region, imaged by the MODIS Airborne Simulator (MAS) 0.67 μm channel, off the coast of Monterey Bay, California on 11 June 1994 from 1730 to 2100 UTC. The cloud boundary, shown in more detail in Fig. 3, is indicated by the arrow. Each ER-2 flight line represents about a 25 minute offset (earlier flight lines to the east) accounting for the discontinuity seen in the cloud boundary between adjacent flight lines.

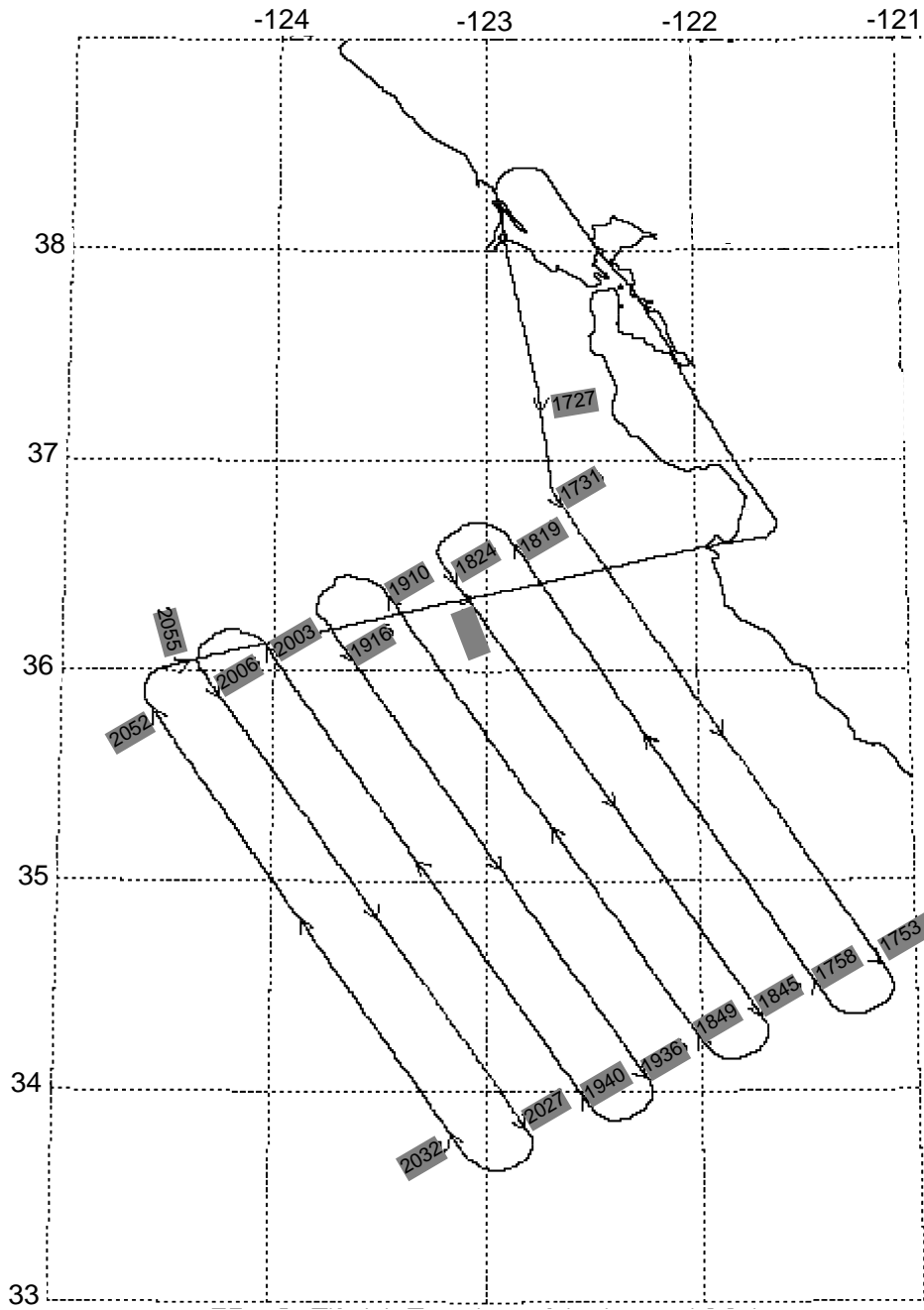


Fig. 2 The flight path of the ER-2 on 11 June 1994 corresponding to the image in Fig. 1. The arrows indicate the direction of travel of the aircraft and the labels refer to the time of overpass in UTC.

↑ Northwest

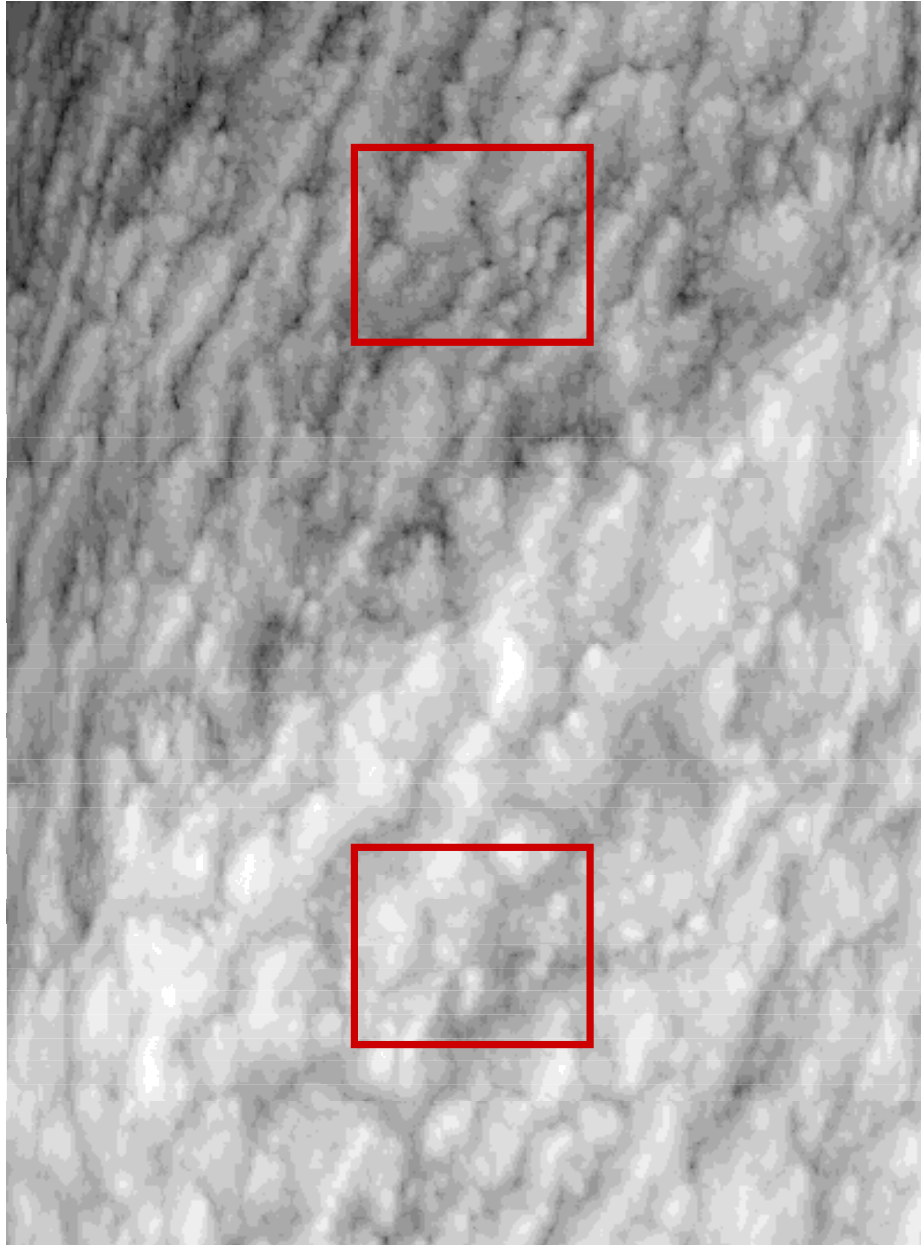


Fig. 3. Cloud boundary imaged with the MAS 0.67 μm channel on 11 June 1994 (ER-2 flight line indicated on Fig. 1). The image area is 35 km across the scan line (horizontal) by about 33 km along the direction of flight (vertical). The image has not been spatially resampled so pixels away from nadir along the scan direction cover larger distances. The regions enclosed by boxes were used for the cloud retrievals discussed in the text.

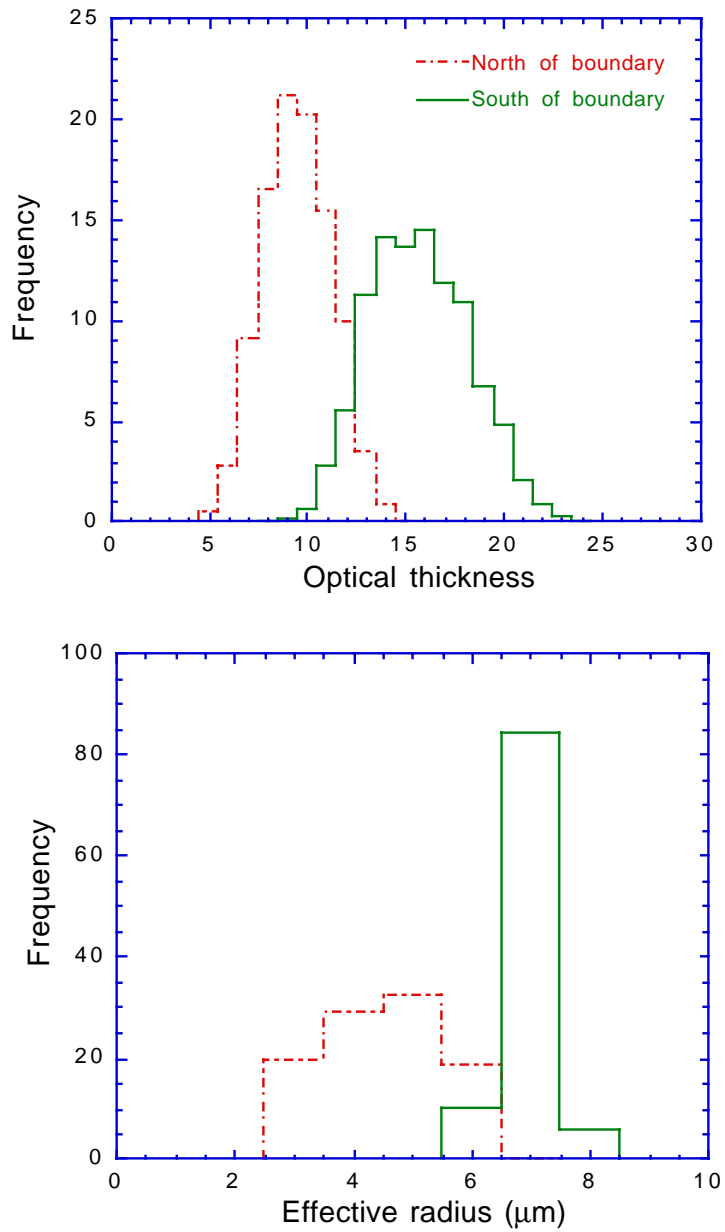


Fig. 4. Retrievals of cloud optical thickness and effective radius made using the MAS 0.67 and 2.13 μm channels on two sides of the cloud boundary shown in Fig. 3, at 2013 UTC. The histograms were generated from retrievals made over regions of about 7.75 km by 5.0 km as indicated by the boxes in Fig. 3.

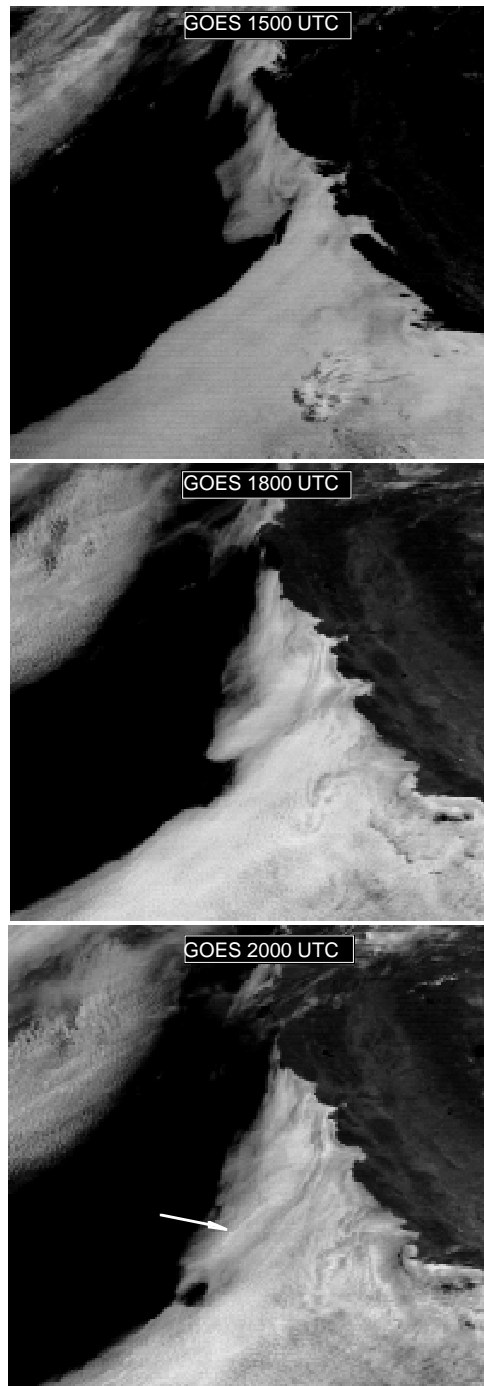


Fig. 5. A sequence of GOES-7 images at 1500, 1800, and 2000 UTC on 11 June 1994 showing the decay phase of the southerly surge. The approximate position of the ER-2 at 2000 UTC is indicated in the image by the arrow.

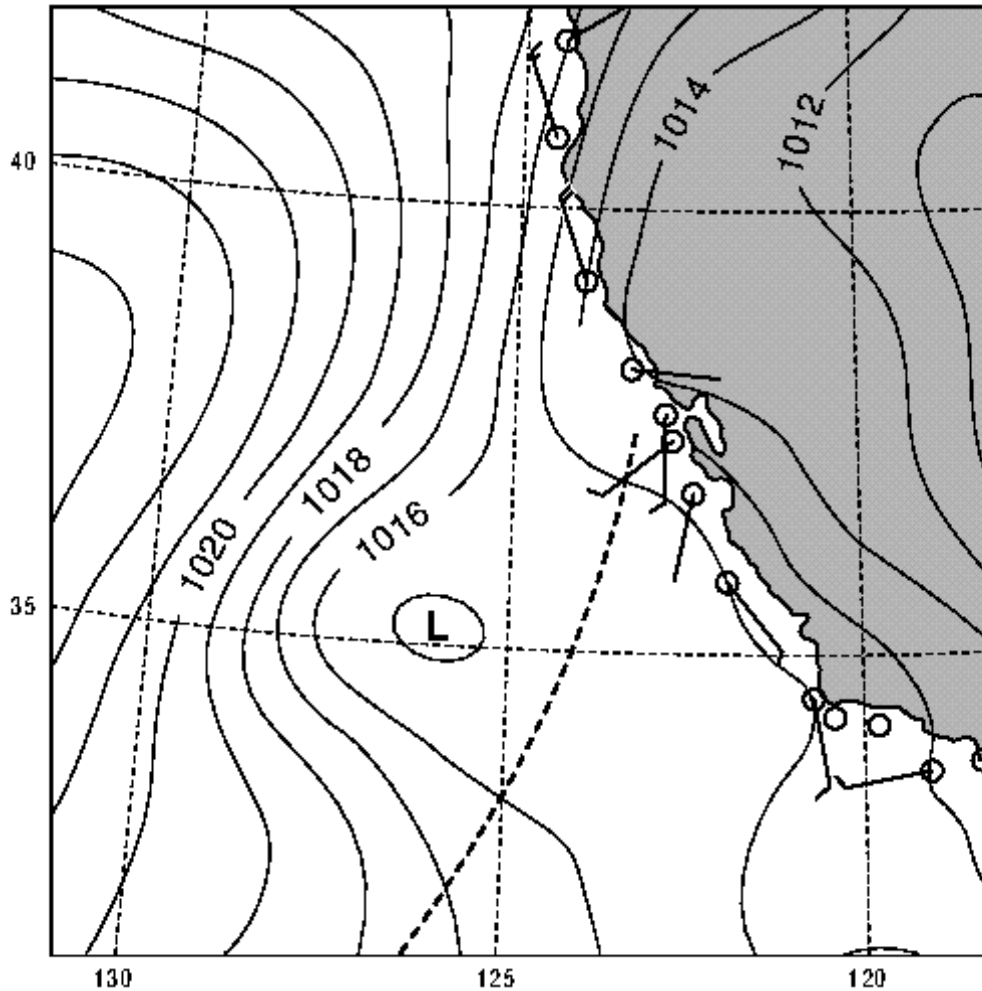


Fig. 6. Isobars of sea-level pressure (solid lines, 1 mb intervals) for 1500 UTC 11 June 1994 near the coast of Monterey Bay, California. The region shown is approximately equal to that in Fig. 5 and the heavy dashed line indicates the approximate eastern edge of the cloud layer visible at 1500 UTC in Fig. 5. Also shown are selected ship and buoy observations of surface wind speed; a full wind barb represents 5 m s^{-1} and a half wind barb 2.5 m s^{-1} . This figure is adapted from Fig. 20 in Oosterling (1995), where more information is given about the multiquadratic technique used to blend available pressure measurements into the gridded fields of the National Meteorological Center mesoscale ETA model.